

1 **Reading the sediment archive of the Eastern Campeche Bank (southern Gulf of**  
2 **Mexico): From the aftermath of the Chicxulub impact to Loop Current variability**

3 Christian Hübscher<sup>1,\*</sup>, Tobias Häcker<sup>1</sup>, Christian Betzler<sup>2</sup>,  
4 Claudia Kalvelage<sup>1,3</sup>, Benedikt Weiß<sup>1,4</sup>

5  
6 *This is a non-peer reviewed preprint*  
7 *submitted to Marine Geophysical Research*  
8

9 <sup>1</sup>University of Hamburg, Center for Earth System Research and Sustainability, Institute of  
10 Geophysics, Bundesstraße 55, 20146, Hamburg, Germany

11 <sup>2</sup>University of Hamburg, Center for Earth System Research and Sustainability, Institute of  
12 Geology, Bundesstraße 55, 20146, Hamburg, Germany

13 <sup>3</sup>Present Address: Die Fähre, Hamburg, Germany

14 <sup>4</sup>Present Address: Bundesamt für Seeschifffahrt und Hydrografie, Hamburg, Germany

15 \*Corresponding author. Email: christian.huebscher@uni-hamburg.de  
16

17 **ORCID:**

18 Christian Hübscher: 0000-0001-6788-7978

19 Christian Betzler: 0000-0002-5757-4553  
20

21 *Declaration of competing interests*

22 The authors declare that they have no known competing financial interests or personal  
23 relationships that could have appeared to influence the work reported in this paper.  
24

25 *Data statement*

26 All M94 seismic data will be uploaded in SEG-Y to PANGAEA data base and will be made  
27 public directly after publication in peer reviewed journal. DOI will be updated during revision  
28 process.  
29

30 *Acknowledgements*

31 We like to thank captain Michael Schneider, his officers and crew of RV METEOR for their  
32 support of ship based working program. We further like to thank Wolfgang Mahrle (German  
33 Federal Foreign Office), Mr. Hubertus von Römer (German Embassy Mexico City) and Mr.  
34 Ansgar Sittman (German Embassy Washington) for their great support during the diplomatic  
35 clearance. Jonas Preine is thanked for proof reading. as well as Chris Lowery and Sean Gulick  
36 for discussions at the early stage of this study.  
37

38 *Funding*

39 RV METEOR expedition M94 was funded by the German Research Foundation (DFG) and the  
40 Federal Ministry of Education and Research (BMBF).

41 *Abstract*

42 This is the first high-resolution seismic study showing how the Chicxulub impact shaped the  
43 eastern slope of the Campeche Bank in the south-eastern Gulf of Mexico. The induced shock  
44 wave fractured Cretaceous strata causing the collapse of the upper slope and shelf over a  
45 length of ca. 200 km. Failed material was either transported downslope or remained in parts  
46 on the accommodation space created by the collapsed. In the Cenozoic, the East Campeche  
47 Plastered Drift developed within the created accommodation space, controlled by the inflowing  
48 surface current from the Caribbean, which forms the Loop Current. The internal reflection  
49 configuration of the drift shows that the closure of the Suwannee Strait in the Late Oligocene  
50 and the closure of the CAS in the Mid to Late Miocene controlled the variability of the southern  
51 Loop Current in time. Since the Loop Current transports heat and moisture from the western  
52 Atlantic warm water pool into the North Atlantic and further to NW Europe by the Gulf Stream,  
53 the drift represents an archive for controlling factors that influenced climate of the northern  
54 hemisphere. This first high-resolution seismic reflection study from the eastern Campeche  
55 Bank expands the understanding of destructive processes that a meteorite impact induces into  
56 the earth system. Furthermore, these data document that the East Campeche Plastered Drift  
57 bears the potential to understand the link between the climate variability of the northern  
58 hemisphere and oceanic processes in the equatorial western Atlantic.

59

60 *Keywords*

61 Marine reflection seismics, plastered drift, deep base level, paleoceanography, meteorite  
62 impact, pockmarks

63

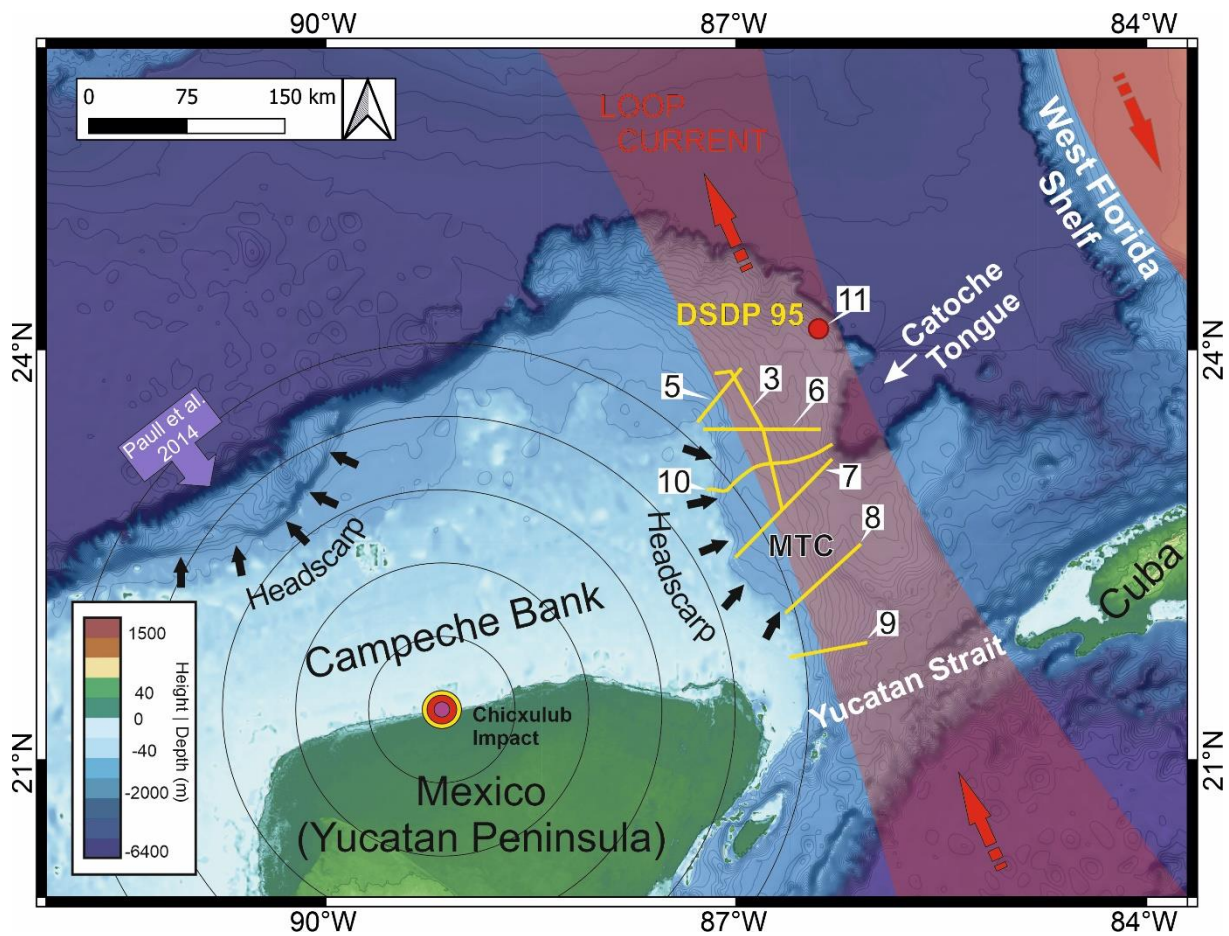
64 *1. Introduction*

65 The impact of the Chicxulub meteorite responsible for the Cretaceous-Paleogene (K-Pg)  
66 extinction event occurred 66 Ma ago on the present-day coastline of Mexico on the northern  
67 Yucatán Platform in the southern Gulf of Mexico (GoM; Fig 1) (Alvarez et al. 1980; Hildebrand  
68 et al. 1991; Schulte et al. 2010). The energy introduced into the Earth system by the impact  
69 was partially converted into a shock wave that would be comparable to the consequences of  
70 a magnitude 11-12 earthquake (Day and Maslin 2005). The shock wave reached the Florida  
71 coast within 4 minutes, triggering surface waves with amplitudes of one meter (Poag 2017).  
72 Portions of the carbonate platforms collapsed, carrying an estimated  $1.98 \times 10^5$  km<sup>3</sup> of  
73 sediment into the Gulf Basin (Sanford et al. 2016). The impact created an elongated, up to 490  
74 m deep basin stretched from the crater to the northern Campeche shelf break, hence  
75 separating the Yucatan Platform in an eastern and western part (Guzmán-Hidalgo et al., 2021).

76 Overall, the K-Pg boundary deposits (KPBD), comprising melt rock, suevite, and lithic impact  
77 breccia, represent the largest mass wasting sedimentary unit of the Earth (Sanford et al. 2016;  
78 Poag 2017) which triggered tsunamis along the GoM (Kinsland et al., 2021). The northern  
79 Campeche Bank, a Cretaceous carbonate platform, is the closest present-day Cretaceous–  
80 Paleogene (K-Pg) boundary outcrop to the Chicxulub impact structure (Paull et al. 2014). The  
81 authors used multibeam data for describing impact related mass wasting due to seismic  
82 shaking produced by the impact. The arcuate steep escarpment face of the northern  
83 Campeche Bank (black arrows in Fig 1) represents the headscarp left behind by extensive  
84 debris flows, which are found in wide areas of the GoM. Hübscher and Nürnberg (2023)

85 proposed that the arcuate escarpment at the eastern Campeche Bank (ECB) represents a  
86 similar headscarp created by Chicxulub impact related mass wasting.

87



88

89

90 *Fig 1 Bathymetric map of southern Gulf of Mexico with adjacent Yucatan and Florida straits.*  
91 *The yellow lines mark the seismic profiles, the label indicate the figure numbers. MTC: mass*  
92 *transport complex. The location of the Chicxulub impact crater is indicated according to Paull*  
93 *et al. (2014). Concentric rings indicate the impact induced seismic wave.*

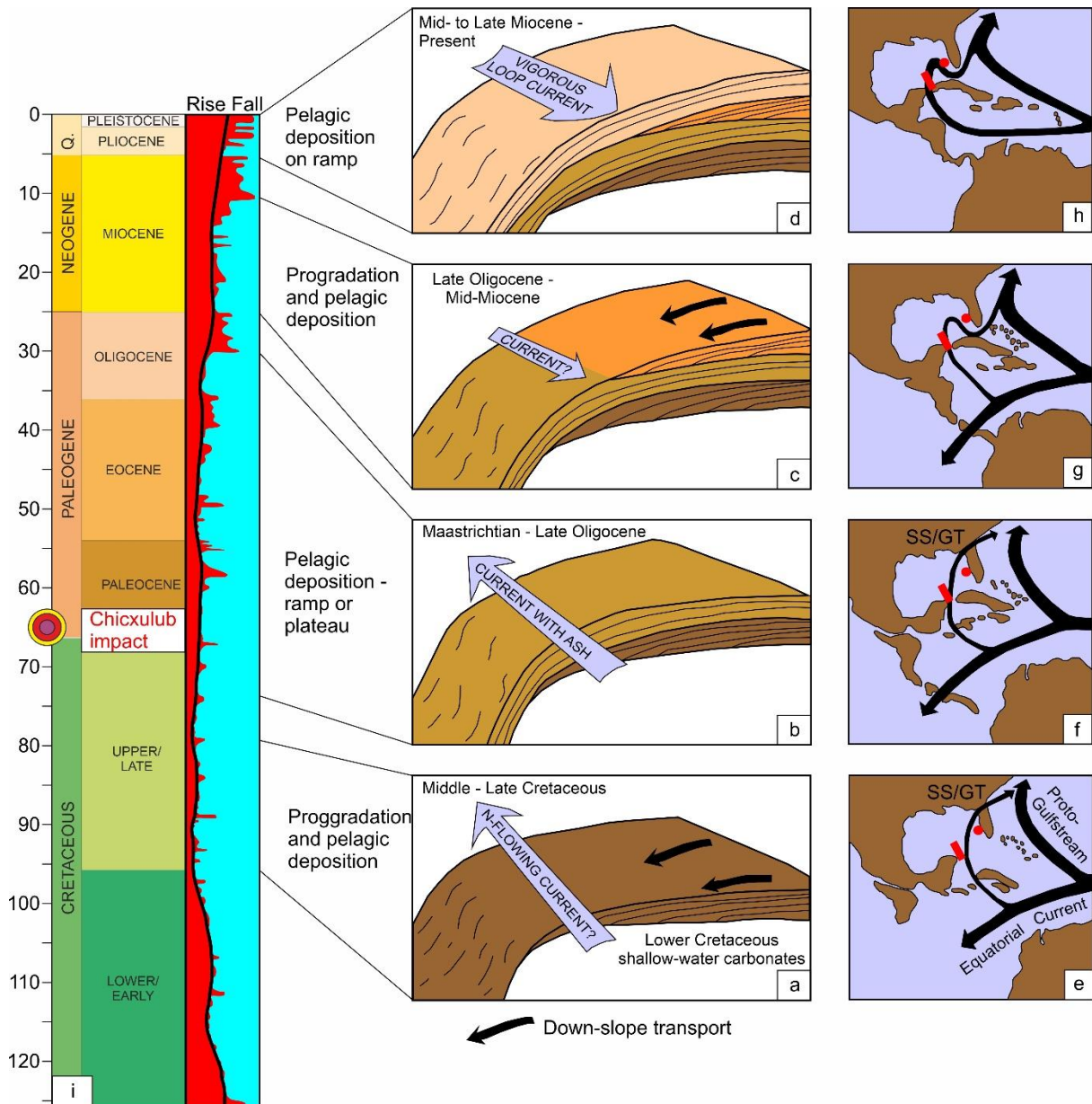
94

95 As summarized by Mullins et al. (1987), ocean currents in the eastern GoM today are  
96 dominated by the Loop Current. This surface current which flows from the Caribbean Sea and  
97 through the Yucatan Strait, streams clockwise into the eastern Gulf and exits into the Atlantic  
98 via the Florida Strait. The surface current then flows northward, where it joins the Antilles  
99 Current northwest of the Bahamas and accounts for about one-third of the total volume of the  
100 Gulf Stream system. Because the Loop Current transports warm tropical water from the  
101 Caribbean to high northern latitudes (Oey 2008 and references therein), its temporal variability  
102 has been an important controlling parameter for Northern Hemisphere climate. Loop Current  
103 variability since the Late Cretaceous has been reconstructed from seismic and  
104 sedimentological data from the western Florida shelf by Gardulski et al. (1991) (Fig 2).  
105 Comparable studies from the conjugate ECB are lacking. This is significant because until the  
106 closure of Suwannee Strait in the late Oligocene to early Miocene, surface flow was northward

107 in both the east and west. Subsequently, the Loop Current formed and the flow along the  
 108 western Florida shelf was southward, in contrast to the eastern Campeche Bank (ECB).

109 In this study, we use high-resolution reflection seismic data measured during RV METEOR  
 110 Expedition M94 (Hübscher et al., 2014) to reconstruct the consequences of the Chicxulub  
 111 impact on the upper slope of the ECB, as well as the influence of the changing oceanic current  
 112 regime like the Loop Current on the deposited sediments after the impact.

113



114

115

116 *Fig 2 Conceptual sketch showing the four major depositional systems identified by Gardulski*  
 117 *et al. (1991) in the context of paleo-circulation (a-h) and eustasy (i). Red dot in paleo-circulation*  
 118 *maps indicate study area of Mullins et al. (1988) and Gardulski et al, (1991). Red rectangle*  
 119 *indicates working area of this study. GT: Gulf Trough; SS: Suwannee Strait.*

120

121

122       2. *Setting*

123    2.1 *Geology of southeastern GoM*

124 Legacy seismic data and cores collected on Leg 77 of the Deep Sea Drilling Project (DSDP)  
125 provide a broad history of the geology of the southeastern GoM (Schlager et al. 1984). Drill  
126 cores from several knolls in the deep southern GoM, i.e., positive bathymetric features with  
127 little overburden over crystalline basement, reveal that Paleozoic basement is comprised of  
128 rifted continental crust (Buffler et al. 1984). The extent and nature of this transitional crust is  
129 still subject of controversy (Kneller and Johnson 2011; Mickus et al. 2009; Pindell and Kennan  
130 2009; Christeson et al. 2014; Eddy et al. 2014; van Avendonk et al. 2015), as no basement  
131 material has been recovered from deep portions of the basin and it is poorly resolved on the  
132 data used by Schlager et al. (1984).

133

134    2.2 *Campeche Bank*

135 The Campeche Bank north of the Yucatan Peninsula (also known as Yucatan Shelf or Yucatan  
136 Carbonate Platform) in the GoM is a carbonate bank which evolved until the mid-Cretaceous  
137 (Ordonez, 1936). It is considered as geologically similar to the southern Florida platform  
138 (Antoine and Ewing, 1963; Uchupi and Emery, 1968). As summarized by Guzmán-Hidalgo et  
139 al. (2021), the Mesozoic and Cenozoic succession comprises mainly carbonate and evaporite,  
140 as well as minor red bed siliciclastic rocks at the base.

141 The Campeche Bank is characterized by a gently dipping seafloor, down to 120 m, followed  
142 by a locally 60 km wide terrace down to ca. 400 m, from where it plunges to 3000 m. Two  
143 submarine terraces (30-36 m, 50 – 63 m) occur in the shallow part, with minor reefs growing  
144 at the position of the deeper terrace (Purser 1983).

145 The lower slope of the northwestern (Site 86), northern (Site 94) and northeastern (Site 96) of  
146 the Campeche Bank has been drilled in the course of DSDP Leg 10 back in 1970 (Fig 2; Worzel  
147 et al. 1973). The results derived from spot coring indicated that the Bank grew as a massive  
148 carbonate platform since Cretaceous times. No evidence for any reef structures or barriers has  
149 been reported. With the exception of Cretaceous dolomite, the recovered sediments were of  
150 deep-water origin (bathyal depths), indicating that the bank has been in the same relative  
151 environment since at least Paleocene or Late Cretaceous. In the context of DSDP Leg 10,  
152 Worzel et al. (1973) interpreted the steep upper slope of the northern Campeche Bank as the  
153 result of upbuilding carbonate sediments. The authors ruled out to see the escarpment as a  
154 fault scarp or as the detrital accumulation seaward of a barrier or reef complex.

155 The Lower Paleocene chinks drilled on close to our study area at Site 95 in a water depth of  
156 1663 m are fractured. Discontinuities in the section and unconformities observed in the seismic  
157 data were interpreted to result from slumping that occurred throughout the Cenozoic along the  
158 ECB slope (Worzel et al. 1973). As it is typical for a ramp, shallow water sedimentary facies  
159 are arranged into depth dependent belts with red and green algae, molluscs, gastropods and  
160 foraminifers down to 80 m, and finer grained deposits in deeper waters (Logan et al. 1969).

161

162    2.3 *Chicxulub Impact*

163 The energy input into the Earth system by the Chicxulub at the Cretaceous-Paleogene (K-Pg)  
164 boundary is estimated to be  $4.2-12 \times 10^{20}$  kJoule (Covey et al. 1994; Hildebrand et al. 1998).  
165 As summarized by Sanford et al. (2016) the subsequent magnitude 11 earthquake generated

166 seismic shaking, ground roll and a mega-tsunami wave train (Kinsland et al., 2021) that  
167 travelled across the gulf within an hour. The resulting debris flows redistributed about  $2 \times 10^5$   
168  $\text{km}^3$  carbonate sediments in the entire GoM, mainly from the Texas shelf and Florida Platform  
169 (Sanford et al. 2016). The redeposited carbonate debris observed in seismic and borehole  
170 data by Sanford et al. (2016) at the Cretaceous-Paleogene boundary has thicknesses on  
171 decimeter and hectometer-scale. Poag (2017) used seismic reflection profiles from the West  
172 Florida Shelf to investigate impact-induced seismic shaking, strata disruption and subsequent  
173 erosion of the Maastrichtian-Campanian depositional sequence.

174 Paull et al. (2014) discussed catastrophic mass wasting along the northern Campeche Bank  
175 due to seismic shaking triggered by the Chicxulub impact (Fig. 1). The gravity flows contributed  
176 to what Paull et al. (2014) called the “K-Pg Cocktail deposits”, comprising melt rock, suevite,  
177 and lithic impact breccia. The mass failure created a rather flat an up to 50 km wide basal  
178 shear surface ramp, on which the Cocktail deposits were deposited, later covered by Cenozoic  
179 post K-Pg event deposits. Guzmán-Hidalgo et al. (2021) showed later, that the flank collapse  
180 at the upper slope of the northern Campeche Bank (Fig 1) occurred at the northern end of the  
181 impact basin that stretches from the shelf break to the crater.

182 The processes important to this study are thus: (1) Within the first seconds to minutes after  
183 impact, seismic ground roll caused sediment liquefaction and internal fracturing of the upper  
184 Cretaceous deposits (Day and Maslin 2005; Poag, 2017). The northern margin of the  
185 Campeche Bank collapsed. (2) Turbidite flows triggered by tsunamis within the first few hours  
186 after impact are deposited in the GoM and Caribbean (Sanford et al. 2016). (3) Carbonates  
187 suspended in the water and iridium-rich ejecta rocks deposited within the first days to weeks  
188 after impact (Sanford et al., 2016). Hübscher and Nürnberg (2023) speculated that the  
189 eastward concave, arcuate rim of the Campeche Bank represents the headwall domain of an  
190 about 150 km broad mass transport complex (MTC), triggered by the Chicxulub impact.

191

#### 192 *2.4 Tectonics, currents and climate*

193 The interaction between tectonics and oceanography north of the Yucatan Strait has been  
194 described for the western Florida shelf (Mullins et al. 1988; Gardulski et al. 1991; Fig 2). After  
195 the mid-Cretaceous drowning of the Florida platform sediment gravity flows caused prograding  
196 deposition under the additional influence of a northbound contour current (Fig 2a, e). Starting  
197 in the Maastrichtian, pelagic deposition of mainly carbonate ooze continued for about 40 Myrs.  
198 (Fig 2b). Until then, the northbound current exited the GoM through the Suwannee Strait  
199 until early Eocene and through the Gulf Trough to late Oligocene (Fig 2e, f). The transition from  
200 Late Cretaceous-Paleogene aggradation to late Oligocene-middle Miocene progradation was  
201 contemporaneous with the infilling and closure of the Suwannee Strait and Florida Trough  
202 during falling eustatic sea level (Fig 2c, g, i) (Gardulski et al. 1991). In the following deposition  
203 took place under the influence of the southward flow of the emerging Loop Current. It should  
204 be noted that this change in flow direction did not affect the ECB to the west.

205 The closure of the Central American Seaway (CAS) caused a significant intensification of the  
206 Loop Current vigor (Fig 2d, h), but the timing of this event is debated. Although the Isthmus of  
207 Panama as a land bridge formed around 2.8 Ma (O’Dea et al. 2016), massive interoceanic  
208 seawater exchange between Atlantic and Pacific ceased by 9.2 Ma due to collision related  
209 uplift (Newkirk and Martine, 2009; Osborne et al., 2014).

210 Subsequently an aggradational ramp developed on the western Florida Shelf above the Mid-  
211 Miocene unconformity (MMU; Mullins et al., 1987; 1988), consisting mostly of calcareous

212 pelagic sediments with some input from the Mississippi River (Fig 2i). Gardulski et al. (1991)  
213 that the strong, southward directed current blocked off-platform transport, because the Loop  
214 Current reached down to the sea floor, e.g. due to the mid-late Miocene sea level fall (Fig 2i).

215 Hübscher et al. (2010) used sediment subbottom profiler data from the southeastern GoM  
216 and discussed the influence of the northbound Loop Current and the counter flow on  
217 sediment drift depositions on the ECB and West Florida Shelf. The data resolved a  
218 prominent unconformity at the upper slope up to 20 m below sea floor which was interpreted  
219 as the consequence of a significant flow change sometime during the Pleistocene. Hübscher  
220 and Nürnberg (2023) interpreted additional hydroacoustic and geological data collected  
221 during RV METEOR expedition M94 (Hübscher et al. 2014) and attributed that unconformity  
222 and its correlated conformity to the Mid-Pleistocene Transition (MPT). The data provided  
223 several indications that the Loop Current weakened after the MPT hence contributing to the  
224 further cooling of the Northern hemisphere. Cold-water corals with drift complexes developed  
225 on the upper slope, first described by Hübscher et al. (2010).

226

### 227 3. *Material and Methods*

228 During RV METEOR expedition M94 in 2013 we collected high-resolution seismic reflection  
229 data by means of two GI-Guns and a short 16-channel analog streamer with a group interval  
230 of 6.25 m (Hübscher et al. 2014). The volume of each GI-Gun was 45 in<sup>3</sup> for the generator with  
231 a 105 in<sup>3</sup> injector volume, both operated in “true GI” mode. The weather conditions were rather  
232 harsh, so noise level was high. The undamped passband of the frequency filter was between  
233 20 and 200 Hz. Further processing steps included predictive deconvolution, spherical  
234 divergence correction, stacking, time-migration, white-noise suppression by the technique  
235 described by Butler (2012) as implemented in Schlumbergers VISTA® processing package  
236 and fx-deconvolution. For more details about the marine seismic method see Hübscher and  
237 Gohl (2014). Additionally, we used vintage seismic profiles GT2-16 and GT3-62 collected in  
238 the course of the Gulf Tectonics projects by the University of Texas Institute for Geophysics  
239 (Buffler 1977; Worzel and Buffler 1978; Dillon et al. 1979). IHS Markit provided the Kingdom®  
240 Geophysics software for data interpretation. The vertical exaggeration which is given for each  
241 seismic figure has been calculated with a constant velocity of 1800 m/s, which is the velocity  
242 that has been estimated by Hübscher and Nürnberg (2023) for upper strata.

243

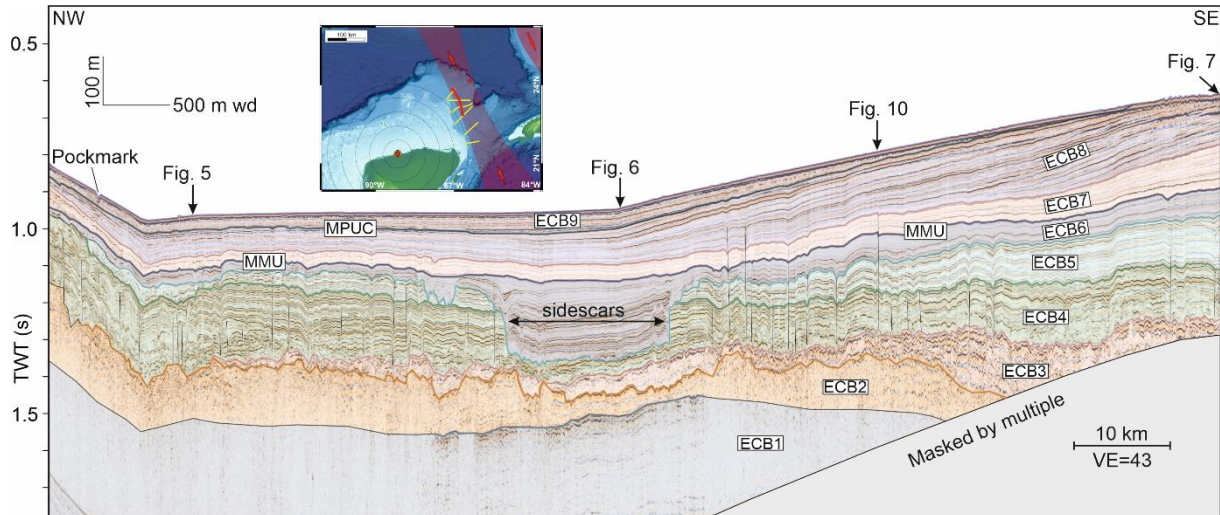
### 244 4. *Observations*

245 As noted already by Hübscher and Nürnberg (2023), the ECB between 22° and 23,5° north  
246 forms a nearly 200 km long arcuate terrain step, which was interpreted as the headscarp of a  
247 mass transport complex (MTC; Fig 1). The upper slope in water depth between 300 m and 600  
248 m reveals a terrace-like morphology. Between 600 m to 1000 m the isobaths are convex-  
249 shaped downslope.

250 In order to set up a seismo-stratigraphic framework we first chose the M94 profile in Fig 3  
251 which runs approximately along the contour and exhibits all the here defined seismic units.  
252 The term "seismic unit" (or simply "unit") is purely descriptive for intervals with similar internal  
253 reflection configurations bounded by unconformities or conformities atop and at their base. The  
254 identified eight units, labelled bottom up ECB1-8 (ECB: East Campeche Bank), are listed and  
255 characterized in Fig 4. The profile in Fig 3 represents also the tie or anchor profile from which  
256 the stratigraphy is extrapolated to the dip profiles in Figs 5-7. No tie lines are available for the  
257 southern two profiles in Figs 8 and 9 which are quite close to the Yucatan Strait (Fig 1), where

258 northbound currents from the Caribbean into the Gulf of Mexico are strongest (Sheinbaum et  
 259 al. 2002). The lower three units can be identified by jump correlation, the units above are  
 260 described in a general way. After establishing the seismo-stratigraphic scheme for the M94  
 261 seismic data, the scheme was projected on the vintage seismic data (Fig 10).

262



263

264

265 *Fig 3 Contour parallel M94 seismic reflection profile. Arrows indicate crossing dip profiles. The*  
 266 *profile location is drawn in the insert map as red line. Seismo-stratigraphic units are labeled*  
 267 *ECB1-9 (East Campeche Bank). MPUC marks the Mid Pleistocene unconformity and*  
 268 *correlated conformity according to Hübscher and Nürnberg (2023). MMU: Mid Miocene*  
 269 *Unconformity.*

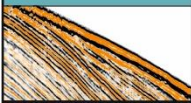
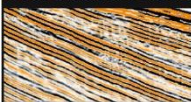
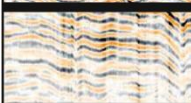
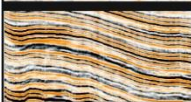
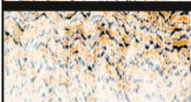
270

271 The lowest unit ECB1, identifiable in the profiles of Figs 3, 6, 9 and 10, exhibits faint subparallel  
 272 and parallel reflections. The upper bounding unconformity is irregular and truncated. The  
 273 resulting ramps have steps of about 100 ms TWT, corresponding to at least 100 m if a p-wave  
 274 velocity of 2 km/s is assumed. The base of ECB1 could not be imaged.

275 The upper boundary of the overlying unit ECB2 represents an irregular or wavy conformity  
 276 where it is not truncated. Internal reflection patches are wavy but discontinuous, other  
 277 segments reveal a chaotic pattern. ECB2 comprises a TWT interval of up to 140 ms,  
 278 representing 140 m if a seismic velocity of 2 km/s is assumed. Unit ECB2 and the units above  
 279 in the MTC terminate upslope against the arcuate headscarp (Figs 5, 6).

280 Chaotic reflections of low amplitudes with some intercalated high amplitude reflections  
 281 characterize unit ECB3, which comprises a TWT interval of up to 60 ms (ca. 60 m). In the  
 282 northern profiles this unit fills up depressions in the top of ECB2 (Figs 5, 6). In the center of the  
 283 MTC, ECB3 is thickest (Fig 7). ECB terminates downslope against a buttress formed by  
 284 ECB1/2 in Figs 7, 9 and 10. In Fig 9, however, ECB3 overran the buttress. In the central part  
 285 of the study area and close to the buttress, internal and partly upslope diverging reflections  
 286 and thrusts are truncated by the overlying unit (Figs 7, 10). As Fig 8 shows, ECB3 is also  
 287 present at the lower slope. No buttress is present here.

288

Seismic Example	Seismic Unit	Reflection Configuration	Stratigraphy	Interpretation
	ECB9	Prograding onlapping clinoform, parallel to divergent, continuous, high amplitude	MPT- Present MPUC	Raising deep base level (Loop Current attenuation)
	ECB8	Prograding, partly offlapping clinoform, parallel to divergent, continuous, high amplitude	MPT- mMio	Falling deep base level (strong Loop Current)
	ECB7	Prograding clinoform, parallel to divergent, continuous reflections of low to medium amplitude		Increasing current control (Loop Current)
	ECB6	Aggrading, subparallel to wavy, continuous reflections of high amplitude	MMU- Mio	Infilling sheeted drift
	ECB5	Prograding, subparallel to wavy, continuous reflections of low amplitude	uOI- Mio	No to little current control, off-bank transport
	ECB4	Aggrading, subparallel to wavy continuous reflections of high amplitude	Pa-uOI	No to little current control, no off-bank transport
	ECB3	Mainly low amplitudes, chaotic, some intercalated high amplitude reflections	K-Pg	Remobilized by L-Pg impact ('K-Pg cocktail')
	ECB2	Wavy patches or chaotic, low to medium amplitudes, discontinuous	uK	Overprinted, fractures by K-Pg impact ('shaken and stirred')
	ECB1	Subparallel, aggrading and continuous, medium amplitudes, upper boundary truncated	IK	Carbonate platform

289

290

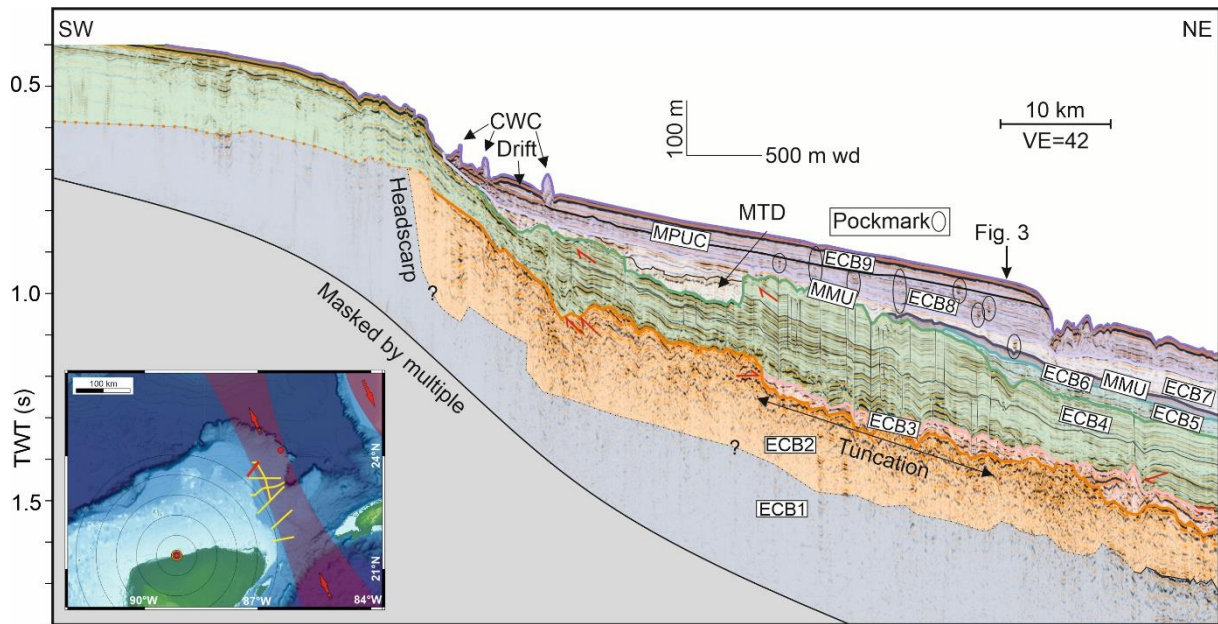
291 *Fig 4 Overview about seismo-stratigraphic scheme. IK: Lower Cretaceous; uK: upper*  
 292 *Cretaceous; Pg: Paleogene; Pa: Paleocene; uOI: upper Oligocene; Mio: Miocene; mMio:*  
 293 *middle Miocene; MMU: Mid-Miocene Unconformity; MPT: Mid-Pleistocene Transition; MPUC:*  
 294 *Mid-Pleistocene Unconformity / Conformity.*

295

296 ECB4 reveals continuous and subparallel to wavy reflections of high amplitude, which build a  
 297 mainly aggrading unit. The maximum TWT interval of up to 200 ms may represent a thickness  
 298 of 200 m or less. If 1.8 km/s, which Hübscher and Nürnberg (2023) calculated for the upper  
 299 strata, are taken for depth conversion, the 200 ms TWT correspond to 180 m. ECB5 and ECB6  
 300 overly ECB4 over wide areas concordantly. However, some areas are truncated or missing  
 301 (Figs 3, 5, 6, 10). In the slope parallel profile (Fig 3) over 17 km in length, the upper ca ¾ part  
 302 of unit ECB4 are eroded. The side walls of the erosional feature are near vertical. The dip  
 303 profile in Fig 6 across this depositional gap shows that unit ECB4 is rather thin if compared to  
 304 the profiles to the north and south. In the same profile, unit ECB4 thickens again where the  
 305 slope forms an almost horizontal plateau.

306 The internal reflection configuration of ECB5 is similar to that of ECB4, but reflection  
 307 amplitudes are generally lower compared to ECB4, and it reaches its maximum thickness on  
 308 the upper slope and in Fig 7, where ECB5 is prograding. North and south of the profile in Fig

309 7, unit ECB5 is either absent or condensed, which means it is too thin to get resolved by the  
 310 seismic data.

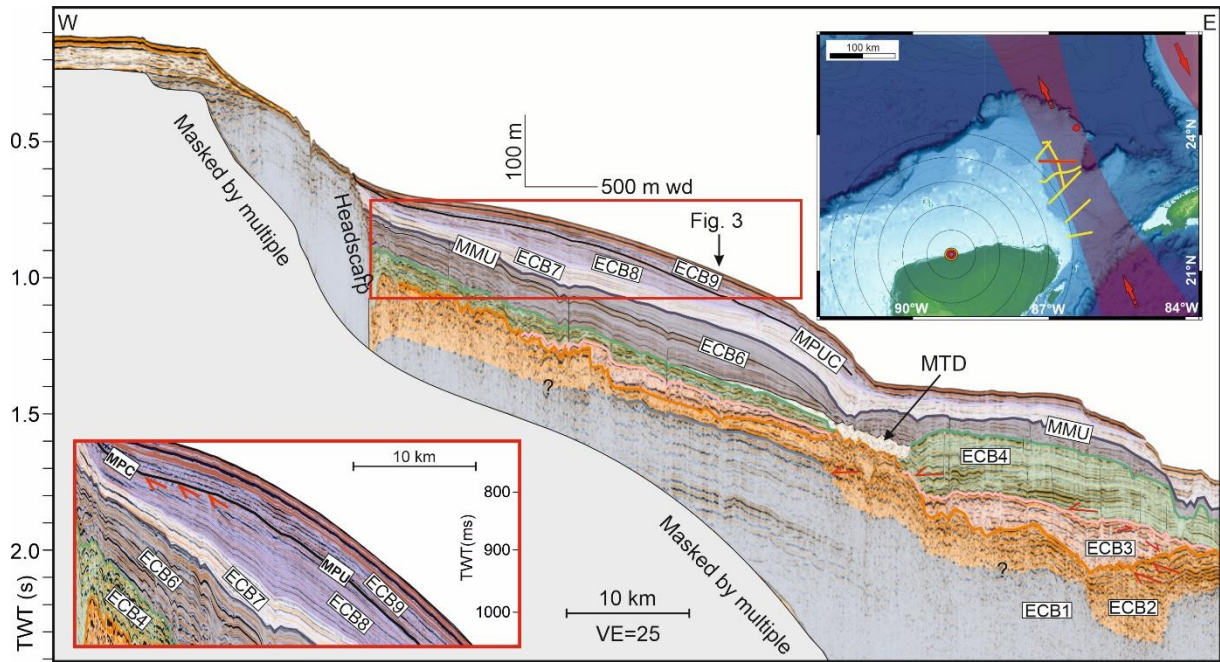


311  
 312  
 313 *Fig 5 Northernmost M94 seismic reflection profile outside the ECPD (East Campeche*  
 314 *Plastered Drift). Cold-water coral (CWC) and the small drift according to Hübscher et al. (2010).*  
 315 *The profile location is drawn in the insert map as red line. The black arrow marks the crossing*  
 316 *location of profile in Fig. 3. MTD: Mass transport deposit. For other abbreviations see Fig. 3.*

317  
 318 ECB6 is aggrading. Internal reflections are subparallel to wavy. ECB6 fills the missing ECB4  
 319 packages (Fig 3, 5, 6) and comprises up to ca. 200 ms TWT (ca. 180 m) where it fills the  
 320 eroded of ECB3 in Fig 3. The upslope termination of ECB6 is truncated in a water depth of ca.  
 321 350 m (400 ms TWT). Near-vertical faults, possibly just narrow folds if considering the limited  
 322 lateral resolution, are abundant within unit ECB4, some of them correlate downwards with the  
 323 top of the underlying unit ECB3 (Fig 5-7), other propagate into units ECB5 or ECB6.

324 Internal reflections of the prograding clinoforms deposits of ECB7 are continuous and parallel  
 325 to divergent. The reflection amplitudes are low to medium. Its thickness may increase (Fig 5)  
 326 or decrease (Fig 7) downslope. In Fig 7, the upslope end of ECB7 is truncated at ca. 350 m  
 327 (450-500 ms TWT).

328



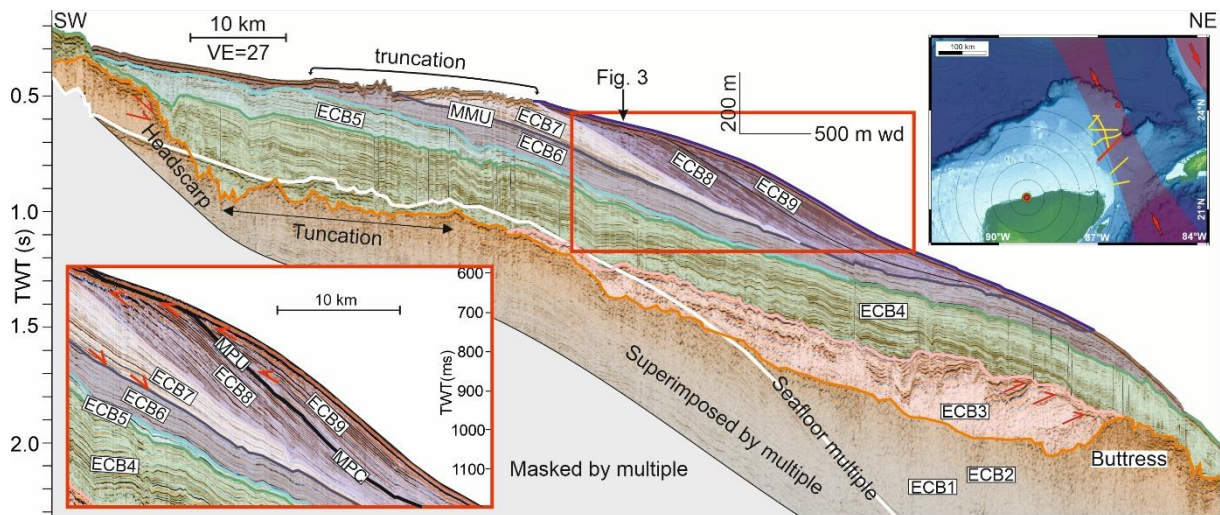
329

330

331 *Fig 6 M94 seismic reflection profile across the northern end of the ECPD. The profile location*  
 332 *is drawn in the insert map as red line. Red arrows mark reflection terminations. The black arrow*  
 333 *marks the crossing location of profile in Fig. 3. MTD: Mass transport deposit. For other*  
 334 *abbreviations see Fig. 3.*

335

336



337

338

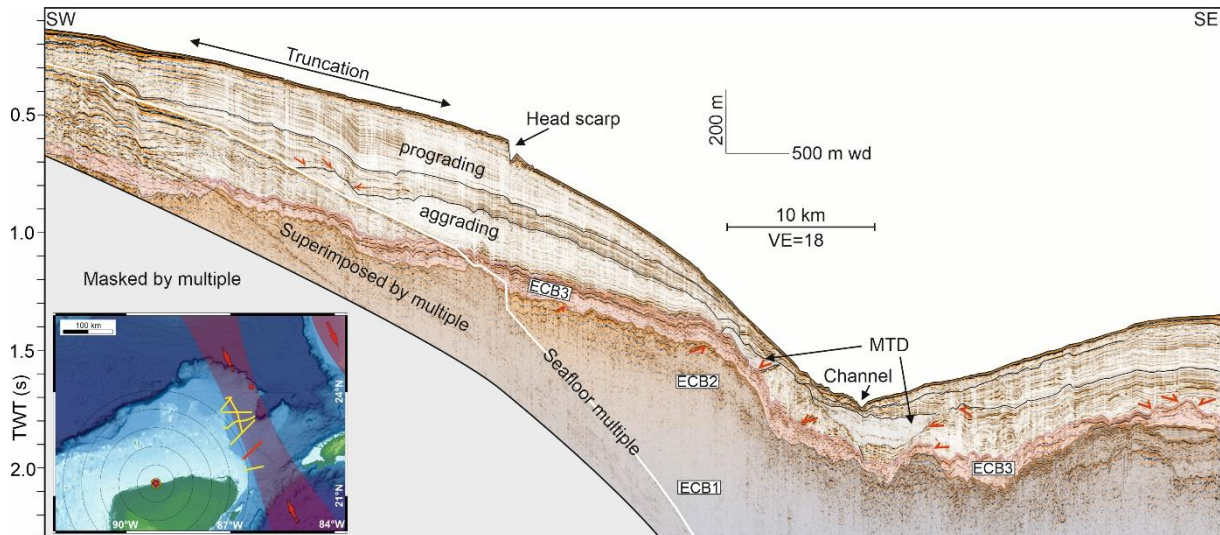
339 *Fig 7 M94 Seismic reflection profile across the central ECPD. The profile location is drawn in*  
 340 *the insert map as red line. The black arrow marks the crossing location of profile in Fig. 3. Red*  
 341 *arrows mark reflection terminations. For other abbreviations see Fig. 3.*

342

343

344 The appearance of ECB8 varies along slope. In the northernmost profile (Fig 5), the internal  
 345 reflections are straight and slightly diverging downslope, and some small depressions are  
 346 intercalated. Reflection amplitudes within these depressions are higher than beside of them.  
 347 Along this profile, ECB8 thickens from ca. 90 m (100 ms TWT,  $v=1.8$  km/s) to ca. 180 m (200  
 348 ms TWT,  $v=1.8$  km/s). In Figs 6 and 10, unit ECB8 represents a ca. 90 m thick (100 ms TWT,  
 349  $v=1.8$  km/s) mounded structure at the upper slope. In Fig 7, unit ECB8 forms sigmoidal  
 350 clinoform with offlapping, down stepping reflections. Here, ECB8 reaches its maximum  
 351 thickness of ca. 200 m (220 ms TWT,  $v=1.8$  km/s).

352



353

354 *Fig 8 M94 seismic reflection profile across the southern ECPD. ECB1-3 are identified from*  
 355 *jump correlation. MTD: Mass transport deposit. The profile location is drawn in the insert map*  
 356 *as red line. Red arrows mark reflection terminations. For other abbreviations see Fig. 3.*

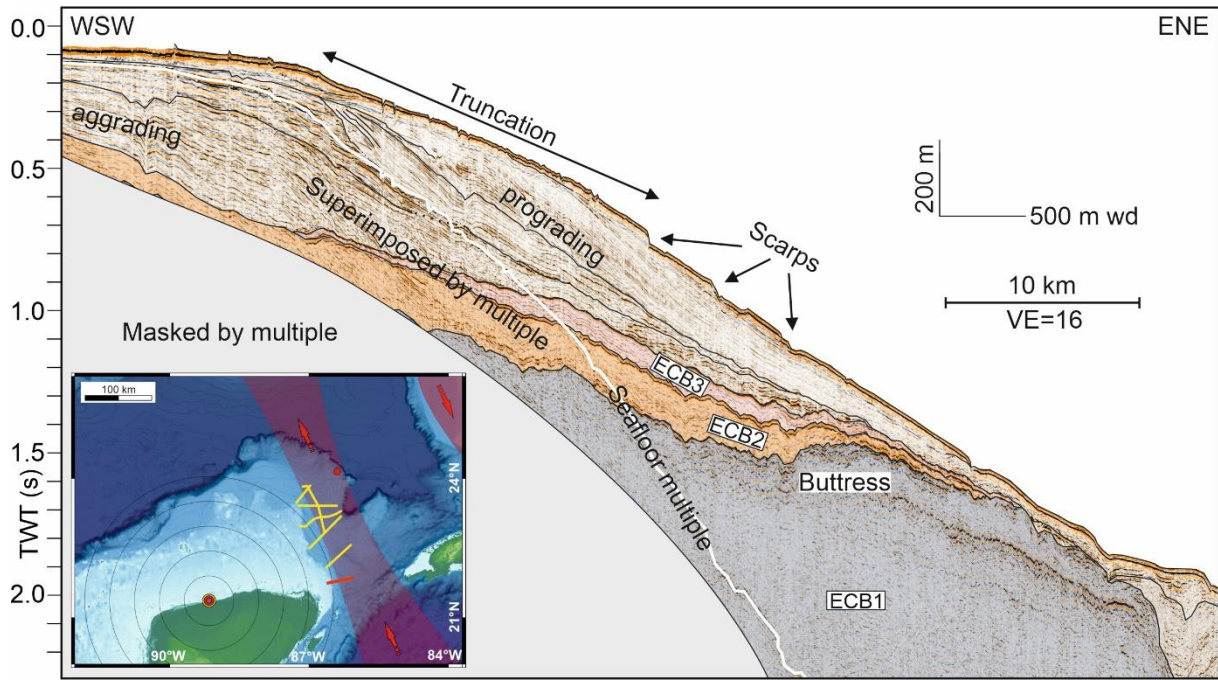
357

358 Unit ECB9 is separated from ECB8 by the Mid Pleistocene unconformity and correlated  
 359 conformity (MPUC), which has been described with sediment subbottom profiler data in  
 360 Hübscher and Nürnberg (2023). The M94 seismic data resolve MPUC and unit ECB9 only in  
 361 Figs 5-7. In the northernmost M94 seismic profile, the internal reflections of ECB 9 are parallel.  
 362 The transition from the Mid Pleistocene unconformity (MPU) to the correlated conformity  
 363 (MPC) occurs at 810 ms TWT, marked by the most basinward toplap of ECB8 against the  
 364 MPU (blowup in Fig. 6). Upper ECB9 clinoforms onlap the MPU from 840 ms TWT and above  
 365 in Fig. 7.

366 Since the profiles in Fig 8 and 9 are not linked to the profiles further north by a tie profile, the  
 367 extrapolation of ECB4-8 to these profiles is not possible. However, both profiles reveal the  
 368 transition from aggrading to prograding above unit ECB3. The upper slope is truncated in both  
 369 instances down to 450 m water depth (600 ms TWT,  $v=1.5$  km/s).

370

371



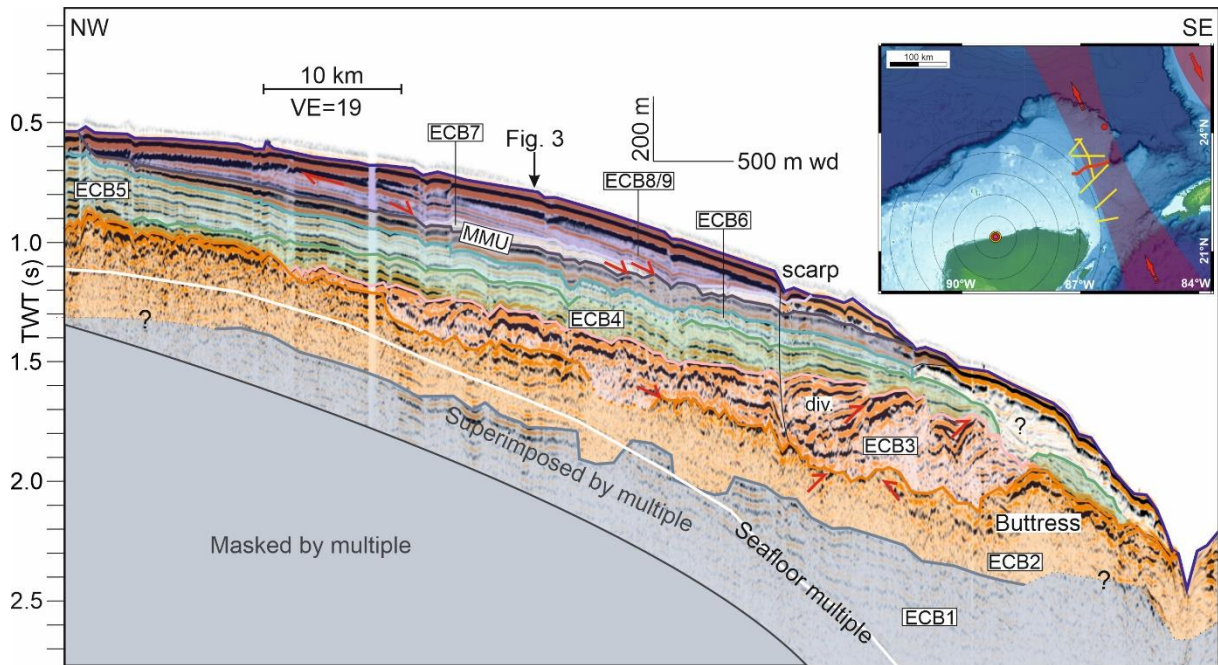
372

373

374 *Fig 9 Southernmost M94 seismic reflection profile south of the ECPD and close to the Yucatan*  
 375 *Strait. ECB1-3 were identified by jump correlation. For other abbreviations see Fig. 3.*

376

377

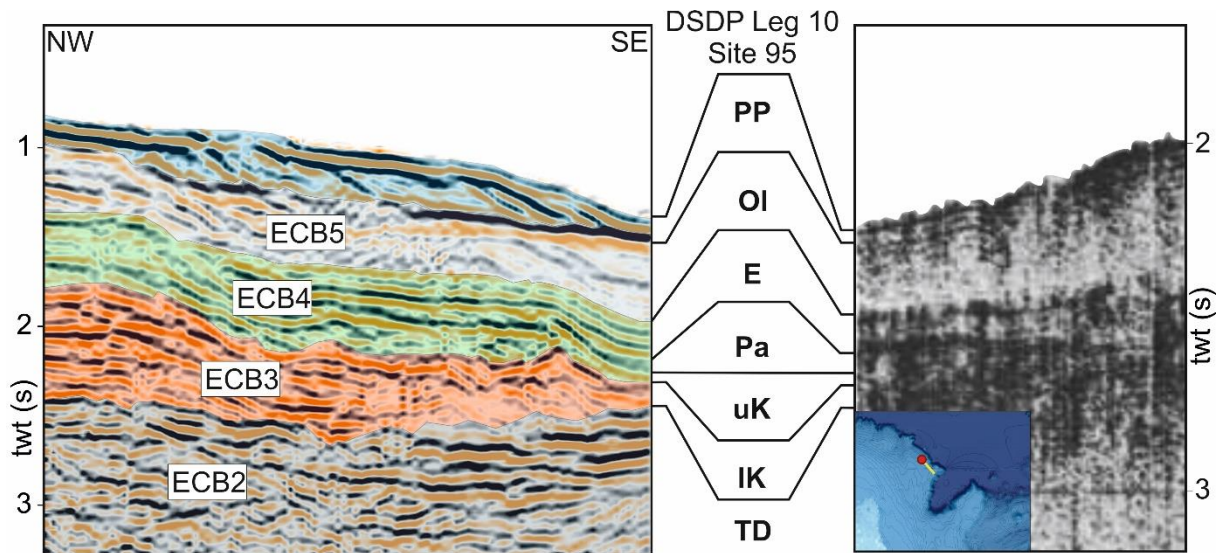


378

379

380 *Fig 10 Vintage seismic reflection profile GT3-62 (Buffler 1977) across the central ECPD used*  
 381 *for jump correlation from DSDP Site 95. The black arrow marks the crossing location of profile*  
 382 *in Fig. 3. For other abbreviations see Fig. 3.*

383



384  
385

386 *Fig 11 Left: Vintage seismic reflection profile GT2-16 (Buffler 1977) crossing DSDP Site 95.*  
 387 *Right: Scan of pre-site survey data for DSDP Site 95 (Worzel et al. 1973). TD: Total Depth; IK:*  
 388 *Lower Cretaceous; uK: Upper Cretaceous; Pa: Paleocene, E: Eocene; OI: Oligocene; PP:*  
 389 *Pliocene-Pleistocene.*

390

## 391 *5 Interpretation and Discussion*

### 392 *5.1 Stratigraphic constraints from DSDP Site 95.*

393 To constrain the stratigraphic interpretation of lower units ECB1-3, two steps were taken. First,  
 394 we scaled the GT2-16 profile and a section of DSDP Site 95 pre-site data (Worzel et al. 1973)  
 395 the same and plotted them against each other (Fig. 11). The quality and vertical resolution of  
 396 the two data are different, so few conclusions can be drawn. One important result is that the  
 397 Cretaceous-Paleocene boundary can be identified and that ECB1-2 corresponds to Lower  
 398 Cretaceous strata and ECB3 to Upper Cretaceous strata. Jump correlation by comparing  
 399 unconformities and internal reflection patterns of the profiles in Figs 10, 11 across the Catoche  
 400 tongue (Fig 1) allows the temporal placement of units ECB1-3 in the ECB.

401 A second jump correlation was required to identify ECB1-3 in the southern profiles (Figs 8, 9)  
 402 of Fig 7. Because the previously described ECB4-8 seismic units exhibit considerable  
 403 variability above 1500 m water depth (2 s TWT), no further correlation is proposed between  
 404 the Cenozoic stratigraphy of Site 95 and the seismic data in Fig. 11.

405

### 406 *5.2 The Campeche Carbonate Platform and the Chicxulub impact*

407 Unit ECB1 represents the acoustic basement and is imaged best in Fig 10. According to DSDP  
 408 Site 95 this unit comprises shallow carbonates of the Campeche Bank. The chaotic and  
 409 discontinuous reflection characteristics of ECB2 corresponds with the Selma-Pine Key  
 410 depositional sequence on the west Florida Shelf (Randazzo 1997), which seismic signature  
 411 Poag (2017) interpreted as the direct consequence of seismic shaking and ground roll by the  
 412 nearby Chicxulub impact. Poag (2017) coined the term “shaken and stirred” for this unit. In  
 413 fact, Worzel et al. (1973) already noted that the Lower Paleocene chalks drilled at Site 95 in a  
 414 water depth of 1663 m are fractured with many of the fractures annealed.

415 The amphitheater like headscarp on the ECB and its similarity to the headscarp at the northern  
416 Campeche Bank (Figs 1, 5, 6, 7) corroborates the interpretation that also the ECB was  
417 structurally overprinted by the impact. When adopting the conceptual model by Paull et al.  
418 (2014; their Fig 5), then it was the seismic wave from the impact that resulted in the collapse  
419 of the ECB ca. 200 km along the platform rim. According to Paull et al. (2014), parts of the  
420 failed material was transported into the basin by gravity flows. Some part of this mass transport  
421 deposits (MTD) remained on the decollement. The abbreviation MTC (mass transport  
422 complex) in Fig 1 refers to the combined MTD deposits on the upper slope within the created  
423 accommodation space and the exported MTD of the lower slope. Unit ECB3 reveals several  
424 characteristics of an MTD (e.g., Bull et al., 2009; and references therein). ECB3 is thickest in  
425 the center of the collapsed ECB (Figs 7 and 10), the reflection pattern is mainly chaotic and it  
426 accumulates upslope of the buttresses in the toe domain as in Figs 7 and 9. In the toe domain  
427 and in the center of the MTD, ECB reveals internal thrusts (Fig 7). We consequently attribute  
428 unit ECB3 to this mass transport deposits, which Paull et al. (2014) called the K-Pg Cocktail.  
429 According to the terminology by Martinez et al. (2005), the MTD is frontally emergent in Figs 8  
430 and 9 where the MTD runs over the buttress, but it is frontally confined in Fig 10. Fig 8 shows  
431 that ECB3 accumulated on the terraces at the lower slope. Hence, ECB3 resembles the  
432 characteristics of the remobilized strata at the northern Campeche Bank.

433 The presence of the “shaken and stirred” unit ECB2 and the K-Pg Cocktail unit ECB3 along in  
434 the northern- and southernmost profiles (Figs 5, 9) and therefore along 240 km along the ECB  
435 rim implies that these deposits are not exclusively present where a major flank collapse  
436 occurred.

437

### 438 *5.3 Post K-Pg Stratigraphy and Paleooceanography*

439 Except for the northern most profile (Fig 5), the sediment deposits along the ECB and above  
440 unit ECB3 form a lenticular, convex sediment body, which is built by aggrading strata in the  
441 lower and basin ward prograding strata in the upper part. According to classification schemes  
442 for drifts units ECB4-9 form a typical plastered drift (e.g., Faugères and Stow, 2008; Rebesco  
443 et al., 2014; and references therein) as already concluded for the mid Pleistocene deposits by  
444 Hübscher and Nürnberg (2023). The infill of the accommodation space that was created by the  
445 Chicxulub impact and the resulting mass wasting can be considered as an infilling drift,  
446 however, since this infilling drift has a continuous transition to the plastered drift to the north  
447 and the south, we refer to this drift as the Eastern Campeche Plastered Drift (ECPD).

448 In order to further constrain the stratigraphic ages of ECB4-9, we compare the reflection  
449 characteristics of individual units with those of the depositional systems on the western Florida  
450 Shelf, where stratigraphic ages were constrained by biostratigraphic markers and volcanic ash  
451 dating (Fig 2; Gardulski et al. 1991).

452 As summarized in Fig 2b, Maastrichtian to Late Oligocene deposits are aggradational on the  
453 West Florida Shelf and so is unit ECB4. Since a significant difference between the current  
454 strength between ECB and Florida is difficult to assume, we relate ECB 4 to the post K-Pg to  
455 Late Oligocene deposits. Aggradational deposition is an evidence for sedimentation in  
456 accommodation space below the deep base level. The term deep base level was coined by  
457 Hübscher et al. (2016) and describes the vertical boundary between erosion and sedimentation  
458 in subaqueous, particularly deep-water environment. The deep base level can be controlled  
459 by, e.g., bottom and contour currents (Hübscher et al. 2016; 2019), surface currents or internal  
460 waves (Qayyum et al. 2017; Hübscher and Nürnberg 2023).

461 When the Loop Current developed after the closure of the Suwannee Strait (Fig 2f) and flow  
462 strength increased due to the narrowing of the CAS, prograding clinoforms developed on the  
463 West Florida Shelf until the Middle Miocene. The surface (Loop) current increase as well as  
464 the Late Oligocene eustatic sea level fall (Fig 2i) caused therewith a relative deep base level  
465 fall that prevented sedimentation above, hence, progradation. This concept does not exclude  
466 enhanced off-bank transport by enhanced carbonate production. At the West Florida Shelf the  
467 prograding clinoforms downlapped on the topset of the Late Oligocene aggradational deposits  
468 on the West Florida Shelf (Fig 2c). At the ECB, the unconformity that marks the transition from  
469 aggradation to progradation separates units ECB4 and ECB5 (Fig 7). Unit ECB6 conformably  
470 overlies ECB5, so we attribute ECB5 and ECB6 to the same time interval from late Oligocene  
471 to Middle-Late Miocene during similar oceanic conditions and constant deep base level depth.

472 In the Middle to Late Miocene, progradational deposition transitioned back to aggradation on  
473 the West Florida Shelf (Fig 2d). Gardulski et al. (1991) attributed this transition to a significant  
474 intensification of the Loop Current when the west-bound current into the Pacific was deflected  
475 by the shallowing of the CAS (Fig 2h). According to these authors, the increased southward  
476 flow hampered significant off-bank transport from the Florida Shelf. The unconformity between  
477 prograding (bottom) and aggrading strata was called the Mid-Miocene Unconformity (MMU)  
478 (Gardulski et al. 1991).

479 The transition from progradation to aggradation is not observed on the ECB. Unit ECB7 marks  
480 a general downslope shift of deposition (Fig 6), a decrease of aggradation and increase in  
481 progradation, and internal reflection terminate as a downlap against its basal boundary (Figs  
482 7, 10). Since an increase in Loop Current vigor should shift the deep base level fall further  
483 down, causing, e.g., non-deposition or truncation in water depth which were previously below  
484 the deep base level, we associate the base of unit ECB7 with the MMU.

485 Since units ECB6 and ECB7 are truncated above ca. 380 m (0.5 s TWT) it cannot be  
486 reconstructed whether these units were previously aggradational further upslope. In the seismic  
487 profile in Fig 7, the offlapping, prograding clinoforms of unit ECB8 resemble the forced  
488 regression systems tract like clinoform that was previously imaged in 4 kHz parametric  
489 sediment echosounder data by Hübscher and Nürnberg (2023).

490 In the northern study area, ECB7 is an upward convex drift deposit (Figs 6, 10). In the central  
491 drift deposition unit ECB7 forms a prograding and sigmoidal clinoform fading out downslope at  
492 1.15 s TWT, which corresponds to ca. 860 m present day water depth (Fig 7). The deep base  
493 level concept explains the different deposition pattern of ECB6 and ECB7. The increasing Loop  
494 Current strength pushed the deep base level down to ca. 520 m, causing erosional truncation  
495 of ECB6 and ECB7 as well as the offlapping clinoforms in Fig 7. The falling deep base level  
496 further explains the progradation and truncation of the upper strata close to the Yucatan Strait  
497 (Figs 8 and 9). Since these seismic units are thinner in Fig 5, 6 and 10 and, hence, located in  
498 deeper water depths, deposition was not affected by the deep base level above.

499 The sigmoidal prograding unit ECB9 in Fig 6 (see blowup) ECB9 overlies the toplapping ECB8  
500 strata, and in Fig 7 the ECB9 strata are onlapping. Both features document a deep base level  
501 rise. This transgressive systems tract like unit overlies the MPUC and developed during the  
502 MPT, implying a weakening of the Loop Current since then (see Hübscher and Nürnberg 2023  
503 for discussion).

504 The here proposed interaction between plate tectonics, oceanic currents and plastered drift  
505 deposition is based on a rather coarse grid of seismic profiles, constrained by jump correlation  
506 between the seismic data from this study and vintage data from the West Florida Shelf where

507 the seismo-stratigraphy was constrained by core data. The lack of in situ age constrains for  
508 the ECB does not allow more detailed conclusions, but the derived explanations are consistent  
509 with finding on the conjugate shelf.

510

#### 511 *5.4 Faults, slumps and pockmarks*

512 Several faults connect to the truncated incisions into the seafloor in Fig 7, which implies that  
513 warping of the strata below is caused by lateral velocity variation or scattering effects, so called  
514 velocity pull-ups or push-downs (e.g., Frahm et al., 2021).

515 Most of the numerous near vertical faults within units ECB4-6 do not propagate to the seafloor.  
516 A plate tectonic origin of those faults is unlikely, which are not connected with deep-rooted  
517 faults. As summarized by Cartwright (2011), those layer-bound faults of a non-tectonic origin  
518 have been observed in 2D-seismic data already in the 1980s (e.g., Buckley and Grant 1985)  
519 and were interpreted as dewatering structures. By using 3D-seismic Cartwright (2004a, b)  
520 showed later that this are polygonal faults, a characteristic that we cannot test with the seismic  
521 lines of this study. Explaining the layer-bound faults purely by dewatering does not explain all  
522 observations. For example, the faults occur more frequently in the upper and lower parts of the  
523 ECPD (Figs 5, 7). Further, Fig 10 shows a scarp at the seafloor, below which a listric fault  
524 extends down into ECB3. Within unit ECB3, divergent reflections and overthrusts are then  
525 seen in the hangingwall domain, which suggest downslope movement. These observations  
526 suggest that the shear strength at the base of unit ECB4 or within ECB3 is so low that minor  
527 downslope creep of unit ECB4, in Fig 7 also within ECB3 occurs, possibly simply triggered by  
528 gravitational forces. If this interpretation holds, the location of dewatering faults in the upslope  
529 domain of the creep would be facilitated by small-scale extension and by compression in the  
530 toe domain. Creep like submarine land sliding in carbonate ooze dominated drift deposits and  
531 along low-angle slopes has recently been shown by Lüdmann et al. (2021). The drift deposits  
532 in the Maldives carbonate platform as discussed by these authors show similar wavy reflection  
533 characteristics, which they attributed to ascending fluids, hence reducing the sediment shear  
534 strength. Also, this explanation is in line with the observations here.

535 The presence of several mass failures in our study, most pronounced in Fig 3 and the  
536 according cross profile in Fig 6, further corroborated the interpretation of reduced shear  
537 strength within unit ECB4. Worzel et al. (1973) concluded already from the interpretation of  
538 DSDP Leg 10 pre-site survey seismic data that slumping occurred throughout the Cenozoic  
539 along the ECB.

540 The small down warped reflections of high reflection amplitude within unit ECB8 in the  
541 northernmost profile (Fig 5) are typical for buried gas escape structures, so called pockmarks  
542 (Hovland and Judd 1988). Multibeam data that were collected along that profile show  
543 pockmarks also on the seafloor (Hübscher and Nürnberg, 2023). Analysis of satellite synthetic  
544 aperture radar mapping showed oils and gas seepage on the sea surface at the southern ECB  
545 (Kennicut 2017), so it is very likely that active hydrocarbons escape started at the ECB during  
546 deposition of units ECB8-9 and the Pleistocene, respectively. Pockmarks on carbonate  
547 platforms has been previously observed, e.g., at the Maldives (Betzler et al., 2011). We can  
548 just speculate that the source rock is part of the Oxfordian (Upper Jurassic) hydrocarbon  
549 system, which according to Hood et al. (2002) is the southernmost source rock in the Gulf of  
550 Mexico. The organic matter deposited during Oceanic Anoxic Events (Schlanger and Jenkyns  
551 1976) may offer be considered as potential sources. The escape of fluids on the sea floor

552 needs further attention, since expelling hydrocarbons may influence water chemistry as well  
553 as flora and fauna habitats (Judd and Hovland 2009; Idczak et al. 2020).

554

## 555 *6. Conclusions*

556 We present the first detailed seismic reflection seismic study of the deep-sea record of the  
557 Chicxulub impact at the K-Pg boundary and the oceanic current controlled depositional  
558 evolution of a plastered drift on the ECB. The seismic wave induced by the Chicxulub impact  
559 caused the collapse of the ECB over a length of ca. 200 km, hence creating accommodation  
560 space for the ECPD. The internal structure of Upper Cretaceous strata was disintegrated. The  
561 failed material was partly transported downslope. Another part remained on the decollement  
562 and formed in dependency of the presence and height of a buttress a frontally confined or  
563 frontally emergent mass transport deposit. The observation of these processes, that were  
564 previously observed at the northern Campeche Bank only, documents the devastating energy  
565 that a meteorite impact induces into the earth system.

566 The closure of the Suwannee Strait in the Late Oligocene and the shallowing and later on the  
567 closure of the CAS in the Mid to Late Miocene controlled the Loop Current variability in space  
568 and time, which in turn controlled the deep base level and therewith the transition from  
569 aggradational to progradational deposition of the ECPD. The deep base level concept proved  
570 to be a useful tool for explaining depositional pattern on continental slope.

571 Since the Loop Current transports heat from the western Atlantic warm water pool into the  
572 North Atlantic, from where heat and moisture is forwarded to NW Europe by the Gulf Stream,  
573 the ECPD represents an archive for the paleoenvironment of the northern hemisphere. The  
574 disclosure of this East Campeche Bank archive needs future attention by interdisciplinary earth  
575 system researchers.

576 *Figure captions*

577 Fig 1 Bathymetric map of southern Gulf of Mexico with adjacent Yucatan and Florida straits.  
578 The yellow lines mark the seismic profiles, the label indicate the figure numbers. MTC: mass  
579 transport complex. The location of the Chicxulub impact crater is indicated according to Paull  
580 et al. (2014). Concentric rings indicate the impact induced seismic wave.

581

582 Fig 2 Conceptual sketch showing the four major depositional systems identified by Gardulski  
583 et al. (1991) in the context of paleo-circulation (a-h) and eustasy (i). Red dot in paleo-circulation  
584 maps indicate study area of Mullins et al. (1988) and Gardulski et al, (1991). Red rectangle  
585 indicates working area of this study. GT: Gulf Trough; SS: Suwannee Strait.

586

587 Fig 3 Contour parallel M94 seismic reflection profile. Arrows indicate crossing dip profiles. The  
588 profile location is drawn in the insert map as red line. Seismo-stratigraphic units are labeled  
589 ECB1-9 (East Campeche Bank). MPUC marks the Mid Pleistocene unconformity and  
590 correlated conformity according to Hübscher and Nürnberg (2023). MMU: Mid Miocene  
591 Unconformity. A clean version of the seismic profile is shown in Fig S1.

592

593 Fig 4 Overview about seismo-stratigraphic scheme. IK: Lower Cretaceous; uK: upper  
594 Cretaceous; Pg: Paleogene; Pa: Paleocene; uOl: upper Oligocene; Mio: Miocene; mMio:  
595 middle Miocene; MMU: Mid-Miocene Unconformity; MPT: Mid-Pleistocene Transition; MPUC:  
596 Mid-Pleistocene Unconformity / Conformity.

597

598 Fig 5 Northernmost M94 seismic reflection profile outside the ECPD (East Campeche  
599 Plastered Drift). Cold-water coral (CWC) and the small drift according to Hübscher et al. (2010).  
600 The profile location is drawn in the insert map as red line. The black arrow marks the crossing  
601 location of profile in Fig. 3. MTD: Mass transport deposit. For other abbreviations see Fig. 3. A  
602 clean version of the seismic profile is shown in Fig S2.

603

604 Fig 6 M94 seismic reflection profile across the northern end of the ECPD. The profile location  
605 is drawn in the insert map as red line. Red arrows mark reflection terminations. The black arrow  
606 marks the crossing location of profile in Fig. 3. MTD: Mass transport deposit. For other  
607 abbreviations see Fig. 3. A clean version of the seismic profile is shown in Fig S3.

608

609 Fig 7 M94 Seismic reflection profile across the central ECPD. The profile location is drawn in  
610 the insert map as red line. The black arrow marks the crossing location of profile in Fig. 3. Red  
611 arrows mark reflection terminations. For other abbreviations see Fig. 3. A clean version of the  
612 seismic profile is shown in Fig S4.

613

614 Fig 8 M94 seismic reflection profile across the southern ECPD. ECB1-3 are identified from  
615 jump correlation. MTD: Mass transport deposit. The profile location is drawn in the insert map  
616 as red line. Red arrows mark reflection terminations. For other abbreviations see Fig. 3. A  
617 clean version of the seismic profile is shown in Fig S5.

618

619 Fig 9 Southernmost M94 seismic reflection profile south of the ECPD and close to the Yucatan  
620 Strait. ECB1-3 were identified by jump correlation. For other abbreviations see Fig. 3. A clean  
621 version of the seismic profile is shown in Fig S6.

622

623 Fig 10 Vintage seismic reflection profile GT3 62 (Buffler 1977) across the central ECPD used  
624 for jump correlation from DSDP Site 95. The black arrow marks the crossing location of profile  
625 in Fig. 3. For other abbreviations see Fig. 3. A clean version of the seismic profile is shown in  
626 Fig S7.

627

628 Fig 11 Left: Vintage seismic reflection profile GT2 16 (Buffler 1977) crossing DSDP Site 95.  
629 Right: Scan of pre-site survey data for DSDP Site 95 (Worzel et al. 1973). TD: Total Depth; IK:  
630 Lower Cretaceous; uK: Upper Cretaceous; Pa: Paleocene, E: Eocene; Ol: Oligocene; PP:  
631 Pliocene-Pleistocene.

632

633

634 *References*

- 635 Alvarez LW, Alvarez, W, Asaro F, Michel HV (1980) Extraterrestrial cause for the cretaceous-  
636 tertiary extinction. *Science*, 208(4448):1095–1108
- 637 Antoine JW, Ewing JI (1963). Seismic refraction measurements on the margins of the Gulf of  
638 Mexico. *J. Geophys. Res.* 68:1975–1996
- 639 Betzler C, Lindhorst S, Hübscher C, Lüdmann T, Fürstenau J (2011) Giant pockmarks in a  
640 carbonate platform (Maldives, Indian Ocean). *Marine Geology*, 289:1-16
- 641 Buckley DE, Grant AC (1985) Fault like features in abyssal plain sediments: possible  
642 dewatering structures. *Journal of Geophysical Research* 90, 9173e9180.
- 643 Bull S, Cartwright J, Huuse M (2009) A review of kinematic indicators from mass-transport  
644 complexes using 3d seismic data. *Marine and Petroleum Geology*, 26(7):1132–1151.
- 645 Buffler RT (1977) Gulf tectonics phase 2. data retrieved from the IDA Green Expedition 2302,  
646 <https://www.marine-geo.org/tools/datasets/28390>.
- 647 Buffler RT, Schleger W, Bowdler JB, Scientific Party (1984) Initial Report of the Deep Sea  
648 Drilling Project, Leg 77. Washington, Scripps institution Oceanography, CA. 77
- 649 Cartwright JA (1994a) Episodic basin-wide hydrofracturing of overpressured early Cenozoic  
650 mudrock sequences in the North Sea Basin. *Marine and Petroleum Geology* 11:587-607
- 651 Cartwright JA (1994b) Episodic basin-wide fluid expulsion from geopressed shale sequences  
652 in the North Sea Basin. *Geology* 22:447-450
- 653 Cartwright J (2011) Diagenetically induced shear failure of fine-grained sediments and the  
654 development of polygonal fault systems. *Marine and Petroleum Geology* 28:1593-1610
- 655 Christeson GL, Van Avedndonk HJA, I.Norton O, Snedden JW, Eddy DR, Karner GD, Johnson  
656 CA (2014) Deep crustal structure in the eastern Gulf of Mexico. *Journal of Geophysical*  
657 *Research* 119:6782-6801
- 658 Covey C, Thompson S L, Weissman PR, MacCracken MC (1994) Global climatic effects of  
659 atmospheric dust from an asteroid or comet impact on earth. *Global and Planetary Change*,  
660 9(3):263–273
- 661 Day S, Maslin M (2005) Linking large impacts, gas hydrates, and carbon isotope excursions  
662 through widespread sediment liquefaction and continental slope failure: The example of the K-  
663 T boundary event. In *Large Meteorite Impacts III*. Geological Society of America.
- 664 Dillon, WP, Paull, CK, Buffler, RT, and Fail, J-P (1979) Structure and development of the  
665 Southeast Georgia Embayment and northern Blake Plateau; preliminary analysis. In: Watkins  
666 JS, Montadert L, Dickerson PW (eds) *Geological and geophysical investigations of continental*  
667 *margins: American Association of Petroleum Geologists (AAPG) Memoir* 29.
- 668 Eddy DR, Van Avendonk HJA, Christeson GL, Norton IO, Karner GD, Johnson CA, Snedden  
669 JW (2014) Deep crustal structure of the northeastern Gulf of Mexico: implications for rift  
670 evolution and seafloor spreading. *Journal of Geophysical Research Solid Earth* 119:6802-  
671 6822.
- 672 Faugères J-C, Stow DAV (2008) Contourite drifts: nature, evolution and controls. In  
673 *Contourites*, Rebesco M, Camerlenghi A (eds), *Developments in Sedimentology* 60. Elsevier:  
674 Amsterdam 257–288

675 Frahm L, Hübscher C, Warwel A, Preine J, Huster H (2020) Misinterpretation of velocity pull-  
676 ups caused by high-velocity infill of tunnel valleys in the southern Baltic Sea. *Near Surface*  
677 *Geophysics* 18(6), 643-657, doi.org/10.1002/nsg.12122

678 Gardulski AF, Marguerite HG, Milsark A, Weiterman SD, Sherwood WW Jr., Mullins HT (1991)  
679 Evolution of a deep-water carbonate platform: Upper Cretaceous to Pleistocene sedimentary  
680 environments on the west Florida margin. *Marine Geology* 101:163-179

681 Guzmán-Hidalgo E, Grajales-Nishimura JM, Eberli GP, Aguayo-Camargo JE, Urrutia-  
682 Fucugauchi J, Pérez-Cruz L (2021) Seismic stratigraphic evidence of a pre-impact basin in the  
683 Yucatán Platform: morphology of the Chicxulub crater and K/Pg boundary deposits. *Marine*  
684 *Geology*, 441, 106594.

685 Hildebrand A R, Pilkington M, Ortiz-Aleman C, Chavez RE, Urrutia-Fucugauchi J, Connors M,  
686 Graniel-Castro E, Camara-Zi A, Halpenny JF, Niehaus D (1998). Mapping chicxulub crater  
687 structure with gravity and seismic reflection data. Geological Society, London, Special  
688 Publications 140(1):155–176.

689 Hildebrand AR, Penfield GT, Kring DA, Pilkington M, Camargo ZA, Jacobsen SB, Boynton WV  
690 (1991) Chicxulub Crater: A possible Cretaceous/ Tertiary boundary impact crater on the  
691 Yucatan Peninsula, Mexico. *Geology* 19(9):867–871

692 Hovland M, Judd AG (1988) Seabed pockmarks and seepages: impact on geology, biology  
693 and the marine environment (Vol. 293). London: Graham & Trotman.

694 Hood KC, Wenger LM, Gross OP, Harrison SC (2002) Hydrocarbon systems analysis of the  
695 northern Gulf of Mexico: Delineation of hydrocarbon migration pathways using seeps and  
696 seismic imaging. In: Schumacher D, LeSchack LA (eds) AAPG Studies in Geology no. 48 and  
697 SEG Geophysical References Series 11:25–40

698 Hübscher C, Dullo C, Flögel S, Titschack J Schönfeld J (2010) Contourite drift evolution and  
699 related coral growth in the eastern Gulf of Mexico and its gateways. *International Journal of*  
700 *Earth Science*, doi https://10.1007/s00531-010-0558-6.

701 Hübscher C, Nürnberg D, Al Hseinat M, Alvarez García M, Erdem Z, Gehre N, Jentzen A,  
702 Kalvelage C, Karas C, Kimmel B, Mildner T, Ortiz AO, Parker AO, Petersen A, Raeke A, Reiche  
703 S, Schmidt M, Weiß B, Wolf D (2014) Yucatan Throughflow - Cruise No. M94 – March 12 –  
704 March 26, 2013 – Balboa (Panama) – Kingston (Jamaica). METEOR Berichte, M94, 32 pp,  
705 DFG-Senatskommission für Ozeanographie, DOI:10.2312/cr\_m94

706 Hübscher C, Gohl K (2014) Reflection / Refraction Seismology. *Encyclopedia of Marine*  
707 *Geosciences*. DOI 10.1007/987-94-007-6644-0\_128-1

708 Hübscher C, Betzler C, Reiche S (2016). Seismo-stratigraphic evidences for deep base level  
709 control on middle to late Pleistocene drift evolution and mass wasting along southern Levant  
710 continental slope (Eastern Mediterranean). *Journal of Marine and Petroleum Geology* 77, 526-  
711 534.

712 Hübscher C, Al Hseinat M, Schneider M, Betzler C (2019). Evolution of Contourite Systems in  
713 the Late Cretaceous Chalk Sea along the Tornquist Zone. *Sedimentology* 66:1341-1360.

714 Hübscher C, Nürnberg D (2023) Loop current attenuation after the Midpleistocene transition  
715 contributes to northern hemisphere cooling. *Marine Geology* 456:106976  
716 <https://doi.org/10.1016/j.margeo.2022.106976>

717 Idczak J, Brodecka-Goluch A, Łukawska-Matuszewska K, Graca B, Gorska N, Klusek Z,  
718 Pezacki PD, Bolalek J (2020). A geophysical, geochemical and microbiological study of a  
719 newly discovered pockmark with active gas seepage and submarine groundwater discharge  
720 (MET1-BH, central Gulf of Gdańsk, southern Baltic Sea). *Science of The Total Environment*,  
721 742, p.140306.

722

723 Judd A, Hovland M (2009) *Seabed fluid flow: the impact on geology, biology and the marine*  
724 *environment*. Cambridge University Press.

725 Kennicutt MC (2017) Oil and gas seeps in the Gulf of Mexico. In: Ward CH (ed.) *Habitats and*  
726 *Biota of the Gulf of Mexico: Before the Deep Water Horizon Spill*, doi 10.1007/978-1-4939-  
727 3447-8\_5. Chapter 5, 275-358

728 Kinsland GL, Egedahl K, Strong MA, Ivy R (2021) Chicxulub impact tsunami megaripples in  
729 the subsurface of Louisiana: Imaged in petroleum industry seismic data. *Earth and Planetary*  
730 *Science Letters*, 570, 117063.

731 Kneller EA, Jackson CA (2011) Plate kinematics of the Gulf of Mexico based on integrated  
732 observations from the Central and South Atlantic, *GCAGS Transactions* 61:283-299

733 Logan BW, Harding JL, Ahr WM, Williams JD, Snead RG (1969) Late Quaternary sediments  
734 of Yucatan Shelf, Mexico. In: *Carbonate sediments and reefs*, vol 11. Yucatan Shelf, Mexico.  
735 AAPG Memoir, pp 5–128

736 Lüdmann T, Betzler C, Lindhorst S, Lahajnar N, Hübscher C (2022) Submarine landsliding in  
737 carbonate ooze along low-angle slopes (Inner Sea, Maldives). *Marine and Petroleum Geology*,  
738 136, 105403. <https://doi.org/10.1016/j.marpetgeo.2021.105403>

739 Martinez JF, Cartwright J, Hall B (2005) 3D seismic interpretation of slump complexes:  
740 examples from the continental margin of Israel. *Basin Res.* 17, 83–108.  
741 <https://doi.org/10.1111/j.1365-2117.2005.00255.xr2005>.

742 Mickus K, Stern RJ, Keller G, Anthony EY (2009) Potential field evidence for a volcanic rifted  
743 margin along the Texas Gulf Coast, *Geology* 37:387-390.

744 Mullins HT, Gardulski AF, Wise Jr. SW, Applegate J (1987) Middle Miocene oceanographic  
745 event in the eastern Gulf of Mexico: Implications for seismic stratigraphic succession and Loop  
746 Current/Gulf Stream circulation. *Geological Society of America Bulletin*, 98:702-713.

747 Mullins HT, Gardulski AF, Hine AC, Melillo AJ, Wise SW, Applegate J (1988) Three-  
748 dimensional sedimentary framework of the carbonate ramp slope of central west Florida: A  
749 sequential seismic stratigraphic perspective. *Geological Society of America Bulletin*, v. 100, pp  
750 514-533.

751 Newkirk DR, Martin E.E. (2009) Circulation through the Central American Seaway during the  
752 Miocene carbonate crash. *Geology* 37:87–90.

753 O’Dea et al. (2016) Formation of the Isthmus of Panama. *Scientific Advances*, 2016, 2(8):  
754 e1600883

755 Oey L, Y (2008) Loop Current and Deep Eddies. *Journal of Physical Oceanography* 38:1426-  
756 1447

757 Ordóñez E (1936) Principal physiogeographic provinces of Mexico. *Am. Assoc. Petrol. Geol.*  
758 *Bull.* 20:1277–1307.

759 Osborne AH, Newkirk DR, Groeneveld J, Martin EE, Tiedemann R, Frank M (2014) The  
760 seawater neodymium and lead isotope record of the final stages of Central American Seaway  
761 closure. *Paleoceanography* 29:715–729

762 Paull CK, Caress DW, Gwiazda R, Urrutia-Fucugauchi J, Rebolledo-Vieyra M, Lundsten E,  
763 Anderson K, Sumner EJ (2014) Cretaceous–Paleogene boundary exposed: Campeche  
764 Escarpment, Gulf of Mexico. *Marine Geology*, 357, 392–400.  
765 doi.org/10.1016/j.margeo.2014.10.002.

766 Pindell JL, Kennan L (2009) Tectonic evolution of the Gulf of Mexico, Caribbean and northern  
767 South America in the mantle reference frame: an update, Geological Society, London, Special  
768 Publications 328:1-55.

769 Poag CW (2017) Shaken and stirred: Seismic evidence of Chicxulub impact effects on the  
770 West Florida carbonate platform, Gulf of Mexico. *Geology* 45:1011–1014  
771 doi:10.1130/G39438.1

772 Purser BH (1983) *Sédimentation et diagenèse des carbonates néritiques récents*, Vol. 2. IFP,  
773 Ed. Technip, 389 pp.

774 Qayyum F, Betzler C, Catuneanu O (2017) The Wheeler diagram, flattening theory, and time.  
775 *Marine and Petroleum Geology*, 86:1417– 1430

776 Randazzo AF (1997) The sedimentary platform of Florida: Mesozoic to Cenozoic. In Randazzo  
777 AF, Jones DS (eds) *The Geology of Florida: Gainesville*, University Press of Florida, pp 39–56

778 Rebesco M, Hernández-Molina FJ, van Rooij D, Wahlin A (2014) Contourites and associated  
779 sediments controlled by deep-water circulation processes: state-of the-art and future  
780 considerations. *Mar. Geol.* 352, 111e154.

781 Renne PR, Deino AL, Hilgen FJ, Kuiper KF, Mark DF, Mitchell III WS, Morgan LE, Mundil R,  
782 Smit J (2013) Time scales of critical events around the Cretaceous-Paleogene boundary,  
783 *Science*, 339(6120), 684–687, doi:10.1126/science.1230492

784 Sanford JC, Snedden JW, Gulick SPS (2016) The Cretaceous-Paleogene boundary deposit in  
785 the Gulf of Mexico: Large-scale oceanic basin response to the Chicxulub impact. *J. Geophys.*  
786 *Res. Solid Earth*, 121:1240–1261, doi:10.1002/2015JB012615

787 Sheinbaum J, Candela J, Badan A, Ochoa J (2002) Flow structure and transport in the Yucatan  
788 Channel. *Geophys Res Lett* 29(3), 1040, doi:10.1029/2001GL013990

789 Schlager W, Buffler RT, Angstadt D, Phair R (1984) Geologic history of the southeastern Gulf  
790 of Mexico. In: Buffler RT, Schlager W, Leg 77 Science Party (es) *Initial Reports of the Deep*  
791 *Sea Drilling Project, Leg 77*. Washington, Scripps institution Oceanography, CA

792 Schulte P., et al. (2010) The Chicxulub asteroid impact and mass extinction at the Cretaceous-  
793 Paleogene boundary, *Science*, 327(5970), 1214–1218, doi:10.1126/science.1177265

794 Uchupi E, Emery KO (1968) Structure of continental margin off Gulf Coast of United States.  
795 *Am. Assoc. Petrol. Geol. Bull.* 52:1162–1193

796 Van Avendonck HJA, Christeson GL, Norton IO, Eddy DR (2015) Continental rifting and  
797 sediment infill in the northwestern Gulf of Mexico. *Geology* 43(7):631–  
798 634, <https://doi.org/10.1130/G36798.1>

799 Worzel J L, Bryant W and Shipboard Scientific Party (1973) Site 95. In: Worzel JL, Bryant W  
800 and Scientific Party, Initial Reports of the Deep Sea Drilling Project, Volume X, Washington  
801 (U.S. Government Printing Office), 259-295

802 Worzel J, Buffler RT (1978) Gulf tectonics phase 3. Data retrieved from the IDA Green  
803 Expedition 2801, <https://www.marine-geo.org/tools/datasets/28447>.

804

805

806